Microprocessors and Microsystems 39.8 (2015): 939 – 949

DOI: http://dx.doi.org/10.1016/j.micpro.2015.10.003

Environment Mapping using a 3D Laser Scanner for Unmanned Ground Vehicles

José-Ignacio Rejas[a], Alberto Sanchez[a,c], Guillermo Glez-de-Rivera[a], Manuel Prieto[b], Javier Garrido[a]

[a] *HCTLab, Univ. Autónoma de Madrid. Francisco Tomas y Valiente 11, Madrid, Spain*
[b] *Robomotion S.L. Parque Científico de Madrid. Campus de Cantoblanco, Madrid, Spain*
[c] *alberto.sanchezgonzalez@uam.es*

Abstract

Unmanned ground vehicles need accurate sensors to detect obstacles and map their surroundings. Laser-based distance sensors offers precise results, but 3D off-the-shelf sensors may be too expensive. This paper presents a 3D sensing system using a 2D laser sensor with a rotation system. Point cloud density analyses are presented in order to achieve the optimal rotation speed depending on the vehicle speed, distance to obstacles, etc. The proposed system is able to generate real-time point clouds, detect obstacles and produce maps, with high accuracy and a reasonable price (less than 5,000 USD).

Keywords:
Laser radar, UGV, 3D mapping

1. Introduction

During last decades, the interest in autonomous and semi-autonomous vehicle navigation is in constant growing. One main application of autonomous vehicles is the transport of humans or goods in conventional roads, but autonomous navigation for UGVs (Unmanned Ground Vehicles) in off-road environments is being also researched by many groups around the world [1, 2]. Unmanned vehicles can be used to explore or map dangerous or unachievable environments by humans. These vehicles are based on sensor measurements to detect obstacles, objects and other environment information to navigate and create models of that environment. Therefore, navigation is a multidisciplinary topic which involves, among others, environment sensing and path planning studies.

Navigation and environment sensing and mapping concepts are not exclusive for unmmaned ground vehicles but also for UUV (Unmanned Underwater Vehicles) [3, 4] and UAV (Unmanned Aerial Vehicles) [5, 6]. A basic component of any unmanned robotic vehicle is the acquisition of exteroceptive models of the environment. The achievement of environment sensing is becoming closer due to the high variety and improvements of the technology. Nowadays, many acquisition systems carry out a sensor fusion approach, which uses different sensing methods to increase the accuracy of the process. This sensor fusion can be performed at different abstraction levels, for example, sensor raw-data level or features level (for example, detection of the obstacle contour) [7, 2]. Sensor fusion can be also applied for indoor navigation [8].

After the acquisition system is defined, navigation should be taking into account. In the literature, many works about unmanned vehicle and robot navigation can be found [9, 10, 11]. Navigation can be based on previously acquired maps, but also mapless navigation can be performed, which is usually necessary in outdoor unstructured environments.

The main goal of this paper is to describe the design of a 3D sensing system for off-road UGVs. A variety of vehicle sensor systems based on different technologies can be found in the literature. These technologies are based on different data acquisition models, which will be briefly explained here:

1.1. Ultrasonic based systems

These sensors are based on the time of flight concept: The ultrasonic waves are emitted, bounced against the objects, and returned to the system.

The distance is calculated measuring the difference of time between the emission time and the reception time, and taking into account the speed of sound.

This technique has been used by indoor robotics [12, 13, 14, 15], but it is not suitable for outdoor applications, because of its directionality, temperature and humidity dependencies, or its dust sensibility and reduced range.

1.2. RADAR (Radio Detecting And Ranging) systems

Radar systems can detect objects and measure the speed and the relative position of them. To achieve this, the system has several antennas transmitting amplitude and frequency modulated waves at high band frequency (tens of gigahertzs). These waves are reflected by the objects located around the radar system, allowing the acquisition of data on a bidimensional space. This type of technology has been used for applications in semi-automatic navigation for unmanned vehicles in pre-established surroundings (highways, roads, etc) [16]. If it is used in unstructured environments, it comes with many problems referring to the detection of some obstacles.

1.3. Systems based on stereoscopic cameras

These systems work in the same way than the human vision. The camera takes two images that are partially overlapped with respect to each other, so a third dimension, i.e. depth, can be calculated, generating the result in a 3D effect. The calibration of the cameras is key to achieve accurate results, because two pictures with different brightness and exposure levels may not be useful. Moreover, this system presents high sensibility to the alignment of the cameras, because a small deviation in it produces wrong depth data calculation. Besides, the distance between both cameras cannot be very small, because too short distances cause geometry deformations, so miniaturization cannot be achieved [17].

Stereoscopic cameras are an especially interesting option if a sensor fusion approach is taken. Besides, this sensing system is very useful in semi-automatic navigation for unmanned vehicles, but it requires heavy data processing. This is because these systems translate the image data to numeric data which represent positions in a map. This technology is used in robots like Curiosity, Spirit [18] and other projects.

1.4. LIDAR systems (LIght Detection And Ranging)

These systems are chosen in a lot of projects dealing with semi-automatic navigation for unmanned vehicles thanks to its great features, such as high speed data acquisition, independence from visibility variations, its accuracy and reliability of the provided data. Most lasers used for LIDAR applications are class 1 laser, which are safe for humans under all conditions of normal use. The Velodyne lasers 3D [19] and Sick lasers 2D [20], among many others, are examples of laser measuring devices.

The data acquisition of a 2D LIDAR system is based on a diode laser that emits its beam toward a rotating mirror, getting a set of points in a bidimensional plane, as it is shown in Fig. 1. To get the 3D effect, a stack of lasers with different orientation angles may be used. Another approach, followed in this paper, implements an additional rotation system to add another axis to the sensing system.

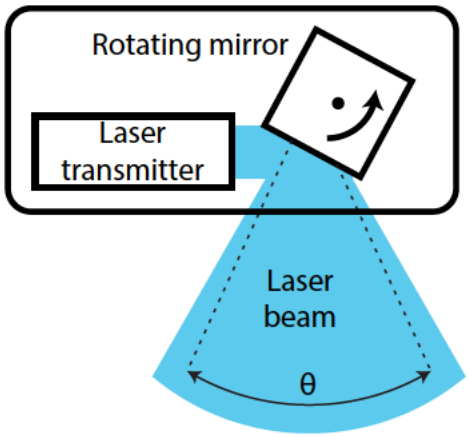

Figure 1: 2D LIDAR scanning laser sensor

Taking into account the different technologies which have been explained, a system based on LIDAR has been chosen, because it offers the following advantages over the other technologies:

- Accuracy in measurements.
- Invariant measures with light intensity. This is a very important parameter for the outdoor case.
- The alignment of the sensor device is not critical.

- Easy configuration of the desired angular aperture, dismissing the kind of data that is not desirable to process.
- Fast data processing.
- Lower rate of false positives than other systems [21].

Navigation for UGVs needs a 3D sensing system. The main problem with 3D LIDAR systems is that they are too expensive (around tens of thousands of USD). Another more economic approach, as it was explained before, is to use a 2D LIDAR sensor and add to it an additional external rotation.

This paper shows how to add this rotation capability to an off-the-shelf 2D sensor. Besides, the paper shows different theoretical studies in order to choose the optimal rotation speed. And finally, the paper shows experimental results.

The rest of the paper is organized as follows. Section 2 describes the sensory system based on a LIDAR approach. Section 3 shows theoretical studies including optimal rotation speed, minimum obstacle size to be detected, etc. Section 4 shows the experimental results of the proposed sensory system. Finally, conclusions are given in section 5.

2. Description of the proposed system

A sensory system is composed of a sensor and a processor to gather all the acquired information and build point clouds of the 3D ranging data. Many studies have been done about obstacle detection and avoidance in outdoor environments, for example [1], in which many LIDAR sensors can be found in a vehicle.

The requirements of an outdoor sensory system are:

- IP (Ingress Protection): The system must be protected against dust and water, as it will be used in outdoor environments. The sensory system must have at least IP 66: Protection against dust and heavy water showers [22].
- Range and aperture: The chosen LIDAR sensor must have a forward measurement range of tens of meters and a customizable aperture of at least 180 degrees, in order to get a clear perception of the environment. Data acquisition of the vehicle front area is specially important because it must be done in real time.
- Accuracy and angular resolution: The sensory system must have an accuracy that allows obstacle detection and avoidance with its data near the vehicle.
- Light intensity: The system must support a light intensity of 100 klux in order to support operation under direct light of the sun.
- Scanning speed: The sensory system should provide fast data acquisition so that it can process and detect obstacles in real time.
- 3D maps generation: The chosen system must be able to acquire and export three-dimensional measurements of the environment in real time in order to generate maps.

Besides, the 3D sensoring system will eventually be applied to navigation of an off-road vehicle. It will support automated decision-making in unstructured environments using data post processing algorithms.

After considering all these engineering requirements, a system based on a 2D laser sensor with a rotating platform is proposed. It is worth to mention that the strategy used in this sensory system has been previously used in other applications [23, 24, 25, 26]. The difference in this case is the laser directionality configuration, the rotation data treatment and its incorporation into a vehicle in order to get a semi-autonomous navigation.

A LIDAR sensor, as it was shown in Fig. 1, emits a laser beam, which is focused to a controlled point by the action of a rotating mirror. When the laser beam bounces in any object, its reflection can be detected with a laser receiver installed in the same sensor. The distance can be inferred applying a time-of-flight approach [14], as it is also used for ultrasonic based systems. When a beam is emitted, a clock counter can be triggered and a reception event stops that counter, see Fig. 2. The time-of-flight can be easily translated to distance taking into account the speed of light, which is not dependent to temperature and humidity. However, in this case, the speed of the laser is much higher than the speed of sound, so more accurate electronics are involved. Another approach is the phase-based measurement, in which the difference between the phases of the transmitted signal and the received signal are compared, as the phase of the transmitted signal is shifted when an obstacle is reached.

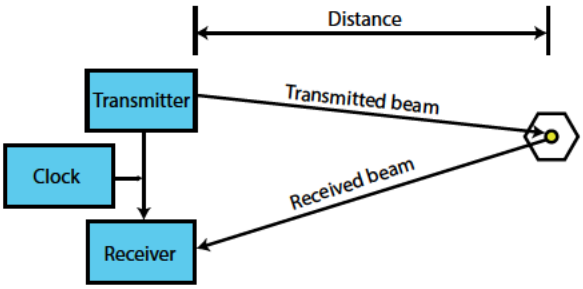

Figure 2: Time-Of-Flight (TOF) laser scanning

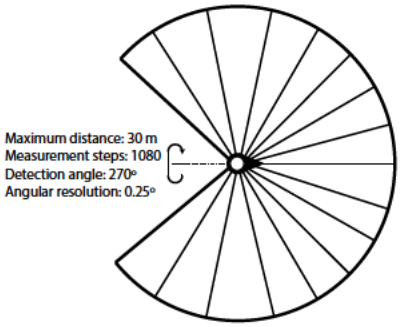

Figure 3: Diagram of scanned area

Phase-based systems are faster and more accurate but they have less range.

In order to design the system, some desirable characteristics for a 2D LIDAR have been chosen, see Fig. 3. Each sweep of the laser has 1080 points, obtained in 25 ms. It has a detection angle of 270°, so the angular resolution is 0.25°. The laser range is 30 m. Doing a simple calculation, the distance between two consecutive points at 30 m inside a sweep can be verified:

$$Resolution = 2\pi \cdot \frac{0.25^\circ}{360^\circ} \cdot 30\ m = 0.1309\ m \quad (1)$$

2.1. Rotation properties

The designed system will rotate continuously a 2D laser sensor around its longitudinal axis, like it is shown in Fig. 4. In the figure, it can be seen the laser beam of the LIDAR sensor (violet area), and the rotation accomplished by the external motor (with a black arrow).

This configuration has been chosen due to the high data redundancy located in front of the laser, namely, more data and more continuously on the obstacles that could be in front of the vehicle. This place is where the detection time is most important.

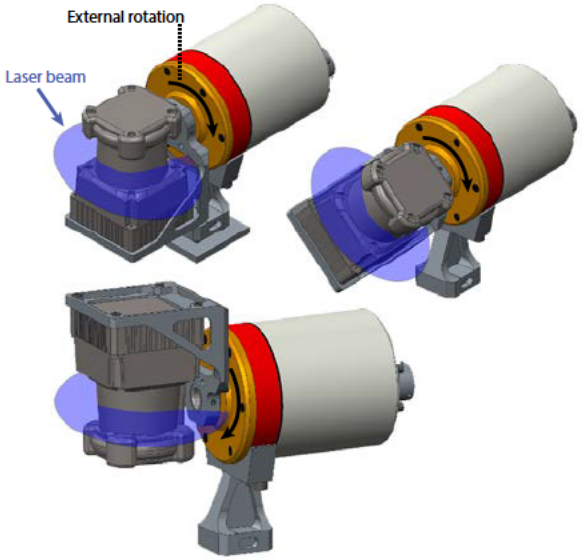

Figure 4: Laser scan with gyro system

Continuous rotation avoids having to stop and start laser motion, so it provides high data rates in a uniform way. However, the system is able to slow down the rotation to acquire more densely populated point clouds in a specific area when necessary.

This system of rotation, while achieving high data redundancy in front of the vehicle, it obtains enough information to detect multiple types of obstacles, negatives as well as positives, that are very important to provide a semi-autonomous navigation. When the sensory system is rotated at least 180°, data redundancy is obtained. With this, and considering the 270° of laser sweep, it is easy to generate a point cloud around vehicle as well.

Now if this rotation method is compared with other articles using laser yaw rotation as for example in [23, 26], it is easy to point out some disadvantages of previous systems when compared to the system proposed in this article. The systems proposed in [23] and [26] do not collect continuously sensory data of the front of the sensor. For instance, in [23] the LIDAR sensor is mounted with the scan plane tilted 45° with respect to the sweep motor axis, as shown in Fig. 5. For semi-autonomous navigation, continuous data acquisition in front of vehicle is necessary, because an accidental collision may happen while the vehicle is moving. This requirement is accomplished in this article.

In [27] no motor-based system is used, but a

tilted-down LIDAR system with a push-broom configuration is used, as seen in Fig. 6. However, this tilt makes shorter the detection range, and collisions with obstacles are more difficult to be avoided, unless the vehicle speed is decreased.

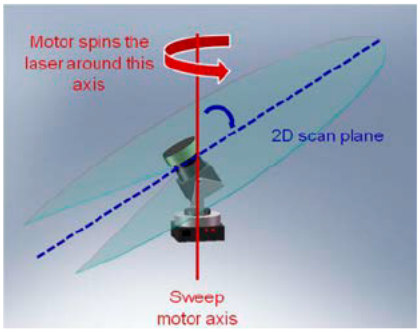

Figure 5: Rotation system used in [23]

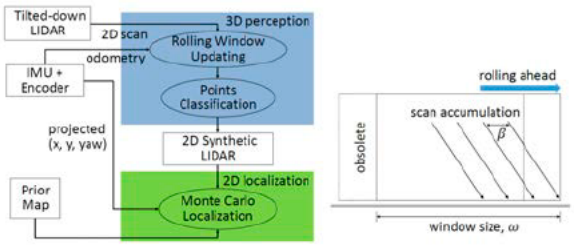

(a) Localization flow chart (b) 3D rolling window

Figure 6: Sensory system used in [27]

Other systems do not turn in a continuous shape, but they make sweeps from side to side. This option is not acceptable because the deceleration of every motor sweep complicates the acquisition of the data with high reliability and accuracy.

Another advantage of the proposed system is that laser scans can be concentrated in a specified region in order to measure with high accuracy and redundancy. The proposed rotation system is composed of the followings components:

- Servomotor: to rotate the laser with controlled rotation angles.
- Encoder: to know accurately the speed and the rotation angle of the motor.
- Inertial Measurement System (IMU): to measure the inclination of the UGV and properly correct the mapping data according to vehicle orientation.

It is important to point out that these components will be installed inside a hermetic body to be protected from water and dust particles from the environment. This way, as it is shown in Fig. 4, the whole system is assembled as only one piece and it is protected against adverse weather conditions.

3. 3D mapping coverage

The rotation speed of the system proposed in the previous section varies the density of the sensed point cloud. Therefore, it is necessary to study the optimal rotation speed depending on the distance to the obstacles, their shape, and the speed of the vehicle as a trade-off with detection resolution. This study is necessary because slow rotation speeds improve resolution at the expense of slowing down the detection of an obstacle, but fast rotation speeds may distort the laser scan and reduce spatial resolutions.

Before starting with the studies, it is necessary to explain with more detail what linear and angular apertures mean. As it was detailed in Fig. 3, the sensor has 270° angular aperture. However, it is usually more useful to delimit the sensed area with a linear aperture, which is equal to the arc length, once known the angular aperture and the sensor distance range. Fig. 7 shows the relation between the angular aperture of the sensor and the linear aperture. As it is shown in the figure, there is an easy relation between the linear aperture and the angular aperture, taking into account the distance between the sensor and the plane that is being analyzed.

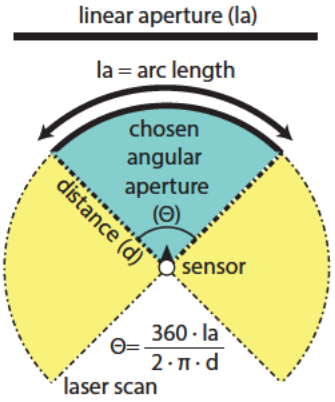

Figure 7: Relation between linear and angular aperture of the sensor

In Fig. 8 the obtained laser geometry at different rotation speeds is shown, where the axis of rotation of the sensory system is centered on the axis center of coordinates. The figure represents a 2D projection of the curved sensed data, which is easier to analyze. In this projection, the horizontal axis represents width distance and the vertical axis represents height distance both in meters.

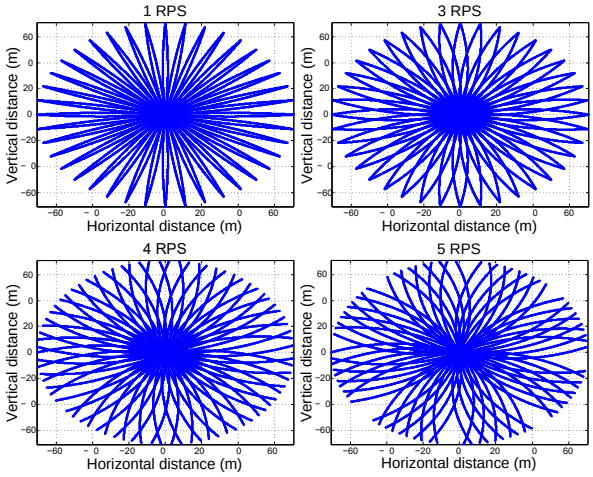

Figure 8: Laser coverage with several rotation speeds for 1 second

For the data analysis, meshing techniques using simulated data have been used to observe the mesh point density generated by the laser at different rotation speeds. To accomplish this, it is necessary to define the minimum cell size taking into account that every cell should have one sensed point.

The following studies will analyze the performance of the system with several sensor apertures (linear and angular aperture), and under different rotation speeds, etc.

3.1. Analysis of the curvature of the laser beam 30 meters away: Static conditions

The external rotation causes the linear laser beam to curve in the measuring space. By continuously updating measured data along linear horizontal and vertical apertures a coverage pattern containing the curved readouts can be studied. Homogeneity is desirable to ensure the sensory system is able to detect geometry features accurately enough in the area of interest.

In Fig. 8 successive full laser scans are shown, corresponding to one second of simulation. Also it can be seen the distortion suffered by the rotation of the laser at different speeds. The objective is to analyze the coverage patterns of laser sweeps depending on the revolutions per second. In this figure, a maximum distance of 30 m in front of the laser can be observed, while the lateral and vertical coverage is delimited by the maximum aperture of the sensor. Applying the calculus seen in Fig.7, the linear aperture at 30 m, with an angular aperture of 270°, is ±70.69 m.

In the previous figure it can be seen that, as the rotation of the system is increased, the laser scanning is more curved. This curvature is produced when the rotation speed of the external motor is close to the internal motor speed of the LIDAR laser. An interesting fact is that homogeneity of the data is lost at 5 RPS and above, because each scanning suffers too many distortions to obtain acceptable density points, so dead zones appear. Therefore, the homogeneity of the data is lost above 5 revolutions per second, in which each laser beam is too distorted to get an acceptable point density. Fig. 9 shows two consecutive laser beams at different speeds between 5 and 8 revolutions per second. At 5 revolutions per second, the sensor would turn 90 degrees in 0.05 seconds, that is two laser scans (every laser sweep lasts 25 ms).

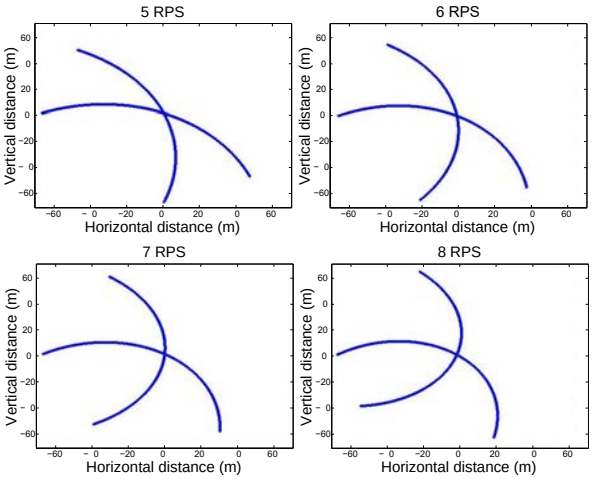

Figure 9: Two consecutive laser beams with several rotation speeds above 5 RPS

3.2. Point cloud coverage density at varying velocities

To better observe the relationship between point density and rotation speed, a constrained linear aperture has been chosen. The chosen linear aperture is ±20 meters in horizontal axis and ±5 meters

Table 1: Meshes (in meters) with different angular apertures

	Angular apertures			
	180°	**90°**	**45°**	**30°**
	1 RPS			
30 m	1.6*1.6	1.6*1.6	1*1.5	1*1
20 m	2*1.5	1.5*1.5	1*1	0.8*0.8
10 m	2*2	0.9*0.9	0.5*0.5	0.3*0.3
5 m	0.8*0.8	0.3*0.3	0.2*0.2	0.1*0.2
	3 RPS			
30 m	1.6*1.4	1.6*1.4	1*1.5	0.8*0.8
20 m	2*1.7	1.6*1.6	0.7*0.8	0.4*0.5
10 m	1.7*1.7	0.9*0.9	0.4*0.3	0.2*0.2
5 m	0.8*0.8	0.3*0.4	0.2*0.1	0.1*0.1
	4 RPS			
30 m	1.6*2	1.6*2	1.1*1.5	0.8*1
20 m	2*1.5	1.7*1.7	0.7*0.9	0.5*0.7
10 m	2.5*2	0.9*0.9	0.4*0.4	0.3*0.3
5 m	1*1	0.3*0.5	0.2*0.2	0.15*0.15
	5 RPS			
30 m	1.6*2	1.6*2	1.6*2	1.3*1.3
20 m	2.3*1.8	1.5*1.6	1.1*1.3	0.9*0.1
10 m	2.5*2.5	0.8*0.9	0.6*0.6	0.5*0.4
5 m	1.5*1.5	0.3*0.5	0.27*0.4	0.2*0.31

in vertical axis. This aperture includes the most important region (front area) for a semi-autonomous navigation in a mobile vehicle system with non-holonomic constraints. Restricting the aperture, the cell size is smaller but the chosen aperture is sufficiently big to sense the desired environment. The cell size is smaller because there is high redundancy in front the of the vehicle, so it is easier that a sensed point is in every cell.

With this configuration, a mesh has been accomplished with a restriction: every single cell will have at least one sensed point. In Table 1, it is represented the simulated meshed values, in meters, for 1 second simulation with different angular apertures (180°, 90°, 45° and 30°) and four rotation speeds.

As an example of these results, for 5 m away and 1 RPS, the minimum cell size for an aperture of 180 degrees is $0.8x0.8$ m. The table shows that at lower speeds, the minimum cell size is smaller, obtaining a better mesh. However, it can be seen that lower speeds do not imply better results. For example, with an aperture of 30 degrees, all the cell size for 3 RPS are better than the results for 1 RPS. As it can be seen, the minimum cell size for 5 m, 180 degrees is equal with 1 and 3 RPS. This is because an angular aperture of 180 degrees covers a big area around the sensor but, as it was explained before, the linear aperture is limited to ±20 and ±5 meters in horizontal and vertical axes respectively.

With these results, it can be seen that there is not a linear relation between speed rotation and minimum cell size. Therefore, a complementary study is required to select the optimum rotational speed in each case, depending on the vehicle speed and the required point density.

3.3. Analysis under dynamic conditions

In a dynamic case, a vehicle has to maintain a guaranteed density reading capability according to vehicle speed and realistic obstacle behavior. Sensor dynamics can thus be adjusted on the fly to meet desirable detection conditions. Therefore, the speed of the vehicle has been taken into account in this section.

Knowing the speed of the vehicle and the time that it gets to stop, it can be estimated the maximum detection time to avoid the obstacle and consider the minimum rotation speed necessary to detect it. The minimum rotation speed has to permit to obtain points in all regions defined in the time established. As the chosen sensor has an aperture of ±135° (Fig.3), only 180 degrees rotation is needed to sense all the space around the vehicle. The results for a vehicle speed of 11 m/s can be seen in Table 2. In the table, it can be seen different distances to an obstacle, and the minimum rotation speed to sense points around all vehicle of the environment.

In Fig. 10 it is shown an example of verification of these minimum values of rotation (see Table 2), in which it can be seen all laser scans accomplished for 0.27 seconds, which is the time until detection (see Table 2), and the mesh generated at each speed of rotation.

Table 2: Time until detection at 11 m/s

Obstacle distance (m)	**Real distance to detect the obstacle (m)**	**Time until detection**	**Minimum RPS**
6	1	0.09	5.555
7	2	0.18	2.75
8	3	0.27	1.85
10	4	0.45	1.11

Simulation results show that at 3 RPS the system is able to obtain data from all regions while at 1.8 RPS it has not turned round enough and, therefore, it has not obtained data from all regions. Rotations above 3 RPS obviously sense all the regions, but the minimum cell is increased.

The selected meshes in Fig. 10 appear in red (±20 m horizontal and ±5 m vertical), and they are going to be adjusted as it was explained before. Table 3 shows the minimum cell size at different rotation speeds. The worst case is considered in

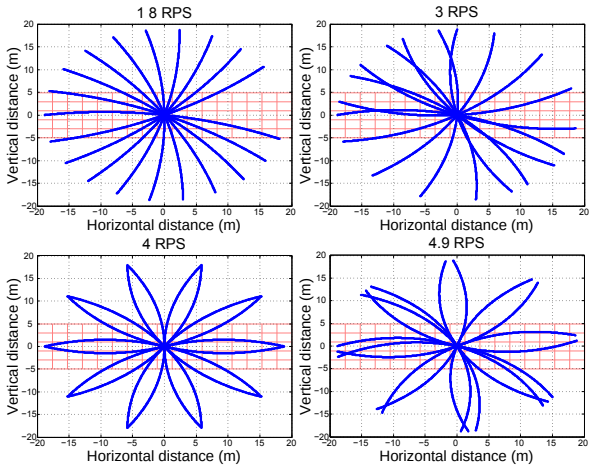

Figure 10: Scans at different rotation speeds with time until detection (speed vehicle: 11 m/s)

this table, so the vehicle is considered to be moving at 11 m/s without any previous data of the sensory system. This situation is more restrictive than a typical real case, because in real situations the sensory system will create point clouds around the vehicle before any move, and it will have some knowledge of the obstacles around. But this theoretical assumption is valid for the case that a dynamic spurious obstacle may arise in a given time.

Table 3: Minimum cell size at different rotation speeds (speed vehicle: 11 m/s)

	Min. mesh (meters) (±20 m,±5 m)	
RPS	**Horizontal axis**	**Vertical axis**
1	>7	>7
1.8	6	6
1.9	4.3	4.3
3	5	5
3.9	4.5	5
4.9	4.5	4.5
5.9	4.5	4.5

Table 3 shows that the minimum cell size at one revolution per second is too big. This is normal as the minimum RPS to cover all the environment in 0.27 seconds is 1.85 RPS (see Table 2). It can be seen that the best result is obtained at 1.9 RPS (above 1.85 RPS) but it does not improve as the rotation speed increases.

Another case of study has been considered, with lower vehicle speed, so there is more time to detect any obstacle. This leads to get more data and therefore the minimum cell size is improved. The results can be seen in Table 4 and 5.

It can be seen again that once the minimum rotation speed is overtaken (<1 RPS in this case), the mesh is not improved if the rotation speed is further increased. Besides, it is important to notice that high rotation speeds involve bigger error in the encoder reading and the synchronization between the encoder data and the laser data. After several additional simulations, it can be deduced that the best mesh is obtained with the minimum rotational speed which assures to sense once all the region around the vehicle. This conclusion may conflict with the idea that the faster the laser turns, the better redundancy and data acquisition environment are obtained.

Table 4: Time until detection at 8.33 m/s

Obstacle distance (m)	**Real distance to detect the obstacle (m)**	**Time until detection**	**Minimum RPS**
6	3.19	0.3823	1.3
7	4.19	0.5023	1
8	5.19	0.6223	<1

Table 5: Minimum cell size at different rotation speeds (speed vehicle: 8.33 m/s)

Mesh (m) (±20 m ±5 m)		
RPS	**Horizontal**	**Vertical**
1	2	2
1.8	2.3	2.3
3	2.5	2.5
3.9	2.5	3.5
4.9	>4	>4
5.9	>>4	>>4

This knowledge has been used to determine sensor rotation speed to achieve a minimum detectable obstacle size for a certain vehicle speed in an area of interest of the road.

3.4. Minimum detectable obstacle and sensor location

Location of the sensor is also important as it will influence the optimal density area along the center of its workspace. The place chosen for installing the sensory system is near the bumper of the vehicle, it is has been set at 1 m above the ground and with a slight down tilt to get maximum surface data density at the road level in front of the vehicle.

Angle of inclination has been chosen to allow detecting an obstacle of 10 cm high and 10 m away from the vehicle, so high point density has been focused at 10 cm from the ground and 10 m away. The tilt angle was calculated to achieve that objective, so it has to detect a conventional curb or step 10 cm high.

The graphs in Fig. 11 show the laser scans for 0.45 seconds, with different rotation speeds and with a mesh of 10 cm in order to verify that it is possible to detect an obstacle of that size at 10 m from the vehicle.

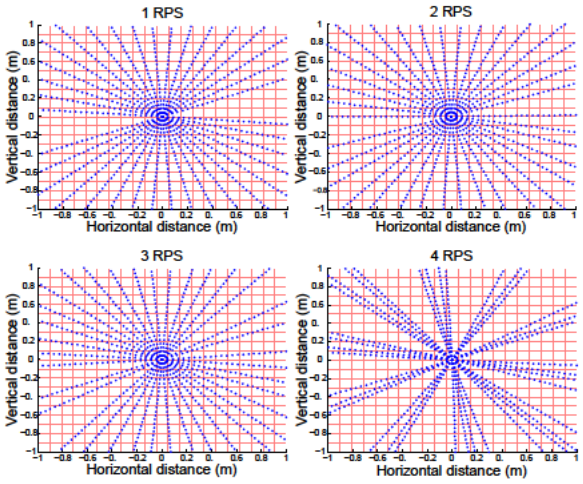

Figure 11: Laser scan configured to detect an obstacle of 10 cm

Results show that the obstacle will always be detected in front of the vehicle even when the coverage pattern depends on the rotation speed.

The system shows properties similar to the human vision where most resolution and detail is obtained in the center of the measurement volume while at the periphery, data is processed at the same rate but with less detail. In case that the system should examine an object at the periphery, the system can decide to focus on it by reducing rotation speed when passing around that area.

In this section, the maximum theoretical rotation speed has been discussed, but it is also necessary to establish a theoretical minimum rotation speed. According to the resolution, i.e. distance between two consecutive points of the same scan, the minimum rotation speed will be calculated so the minimum distance between one point of a scan and the same equivalent point in the next scan is equal to the former resolution. In order to achieve the proposed resolution, the motor rotation angle between two consecutive points can be calculated using the law of sines, as seen in Fig. 12 and the following equation:

$$2 \cdot range = \frac{resolution}{sin(\alpha)}$$

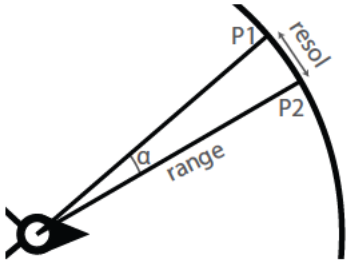

Figure 12: Calculation of rotation angle between two points

$$\alpha = arcsin(\frac{resolution}{2 \cdot range}) \quad (2)$$

In the proposed case, the range is 30 m, and the resolution is 0.1309 m (see Equation(1)), so rotation angle is 0.125°. Once the motor rotation angle is calculated, it can be inferred the rotation speed taking into account the time between two consecutive scans. In the proposed case case is 25 ms (see Fig. 3), so the minimum rotation speed is 0.0139 RPS.

Therefore, the rotation speed must be between 0.0139 and 5 RPS. Those limits are too wide but, thanks to the studies previously presented in this section, the optimal rotation speed can be obtained. To obtain it, some steps must be followed: First of all, the environmental conditions must be considered (at least maximum vehicle speed and maximum dynamic obstacle speed). After that, the worst case must be studied as in section 3.3 was shown. Finally, the optimal rotation speed is the minimum which lets the laser system sense the entire region around the vehicle under the worst imposed conditions.

Our study reflects that the sensor can be operated in different regimes according to resolution and dynamic needs. An optimal rotation speed can always be found so that the laser system covers the region of interest with a desired maximum grid size. This is only limited by physical properties of the sensor itself such as the stated min. 0.25° resolution. For highly dynamic use cases, the sensor may not be able to achieve the most accurate homogeneous grids since it needs to slow down to a minimum 0.25° by 0.25° grid speed.

A prototype of this sensor has been built and experimental results confirm results from the simulation trials presented.

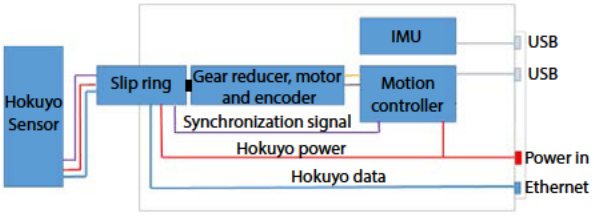

Figure 13: High level architecture of the sensing system

Figure 14: Sensor system based on a 30LX Hokuyo 2D sensor and a rotation system

4. Experimental results

The 3D mapping system has been developed using a 30LX module of Hokuyo [28], which is a time-of-flight based LIDAR system. This module has a detection angle of 270°, an angular resolution of 0.25° and a detection range between 0.1 to 30 m. The high level architecture of the sensing system can be seen in Fig. 13.

As it can be seen in Fig. 13, a slip ring is installed to transmit the power and the data signals between the motor system and the laser sensor, thus ensuring continuous rotation without cable damage. Besides, the sensing system has an IMU (Inertial Measurement Unit) to compensate the orientation and tilt of the sensor, so the 3D maps are correctly composed. The measurement of the orientation and tilt is accomplished using three gyroscopes, three accelerometers and, optionally, three magnetometers. Finally, a closed loop positioning and speed controller is included to read the encoder data and control the motor with high accuracy.

Fig. 14 shows the sensor, the slip ring, and the gear reducer, motor and encoder. The cost of these components is less than 5000 USD.

Simulations of the system have been done using the Gazebo robotics simulator [29] using a computer. In this case, real time is achieved if the computer analysis is accomplished at least at the same speed of the sensory data. Therefore, the computer

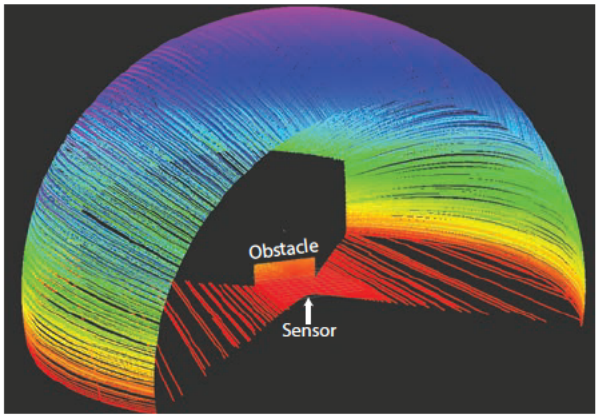

Figure 15: Gazebo simulation of the sensor and an obstacle

should process 1080 points every 25 ms, which is the data rate of the sensor. The proposed system, using a processor Intel i7 running Linux Ubuntu 14.04, is able to create a model of the environment in real time using less than the 60% of the CPU time, including the operating system. A graphical representation of a Gazebo simulation is shown in Fig. 15. In this figure, it can be seen the scanned area around the laser sensor, with an angular aperture of 270°. The simulation shows how the sensor detects a wall-shaped obstacle, and the shadow that the obstacle projects.

As it was seen in section 3, the rotation speed affects the mapping coverage and the update time of a sensed point. As it was explained before, the optimal speed should be inferred taking into account the speed of the vehicle, speed of dynamic obstacles, etc, so it is not unique for all situations. In the experimental results shown in this section, a rotation speed of 1.5 RPS has been selected for testing purposes. This works suboptimally for static cases but gives enough flexibility to use in vehicle speeds up to 5.5 m/s. The system can increase its rotation speed if the vehicle moves quicker.

All the capture and processing stages have been developed using ROS (Robot Operating System) [30]. This robotic-oriented framework provides abstraction layers and multitasking. A ROS-based system splits its functionality into nodes (process) which run independently but they are connected between each other's. The renders of the 3D maps have been built using Rviz [31] and Octovis [32].

In the following subsections, static and dynamic results will be shown.

4.1. Static experiments

The first experiment is an static map of a room which also includes static obstacles, as it can be seen in Fig. 16.

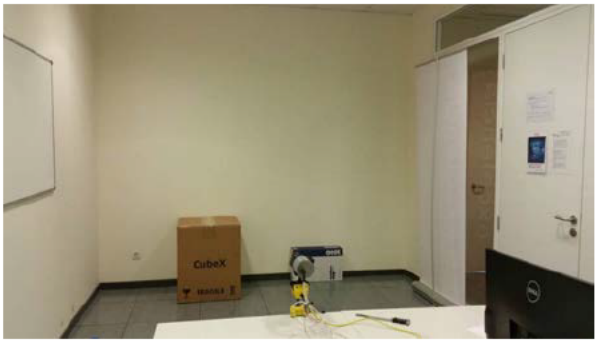

Figure 16: Picture of the sensed room

As it can be seen, the room has a crystal wall partially hidden by a vertical white screen, and two boxes of different sizes in front of the sensor. In Fig. 17 it is shown the 3D map built with Octovis. This Octovis representation has transformed every point in a $5x5$ cm cube.

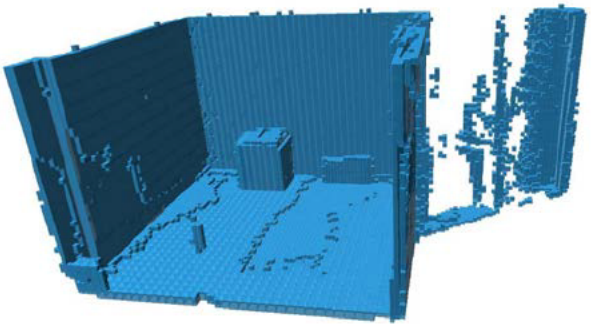

Figure 17: 3D Octovis representation of the room

Fig. 17 shows the boxes correctly sensed. Besides, it can be seen that the system has sensed the space beyond the crystal wall. However, the crystal distorts the acquired data, which can be seen at the right side of the map. In Fig. 18 it can be seen a 2D map which can be helpful to navigation purposes.

Analyzing quantitatively the experimental results, it can be shown that the error in the measure of the left wall is 10 cm (3.12%), and the error in the front wall is 7 cm (2.06%). Different significant points have been analyzed and the error of the sensing system is about 10 cm in average.

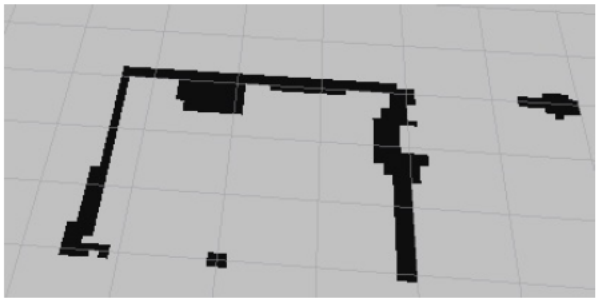

Figure 18: 2D representation of the sensed room

4.2. Dynamic experiments

This subsection includes two experiments: mapping an underground parking with the sensor mounted on a moving vehicle, and the detection of a person moving in front of the static vehicle.

In the first experiment, moving vehicle, the IMU system gains importance because it compensates the orientation changes of the vehicle, so the map is consistent. However, as the IMU cannot offer ideal results, the error in this system produces distortion in the map. Besides, the error of the IMU is cumulative.

Fig. 19 shows a sequence of pictures with the path that the vehicle follows during this experiment, which is an underground parking with a grid of pillars.

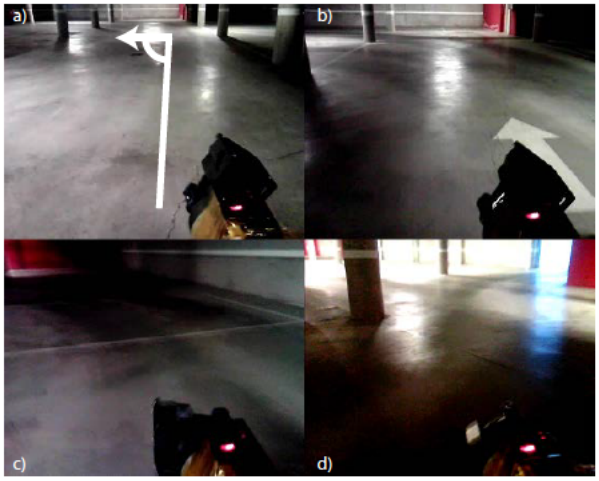

Figure 19: Sequence of pictures of the vehicle path

In Fig. 20, it can be seen the 2D representation of the parking after the mapping process. The vehicle speed has been estimated because at experiment time the vehicle wheel odometer was not present.

Therefore, it can be seen that the pillars are distorted in the 2D representation, but the system produces a suitable map. If a speed meter were installed, most of the produced distortion would be removed.

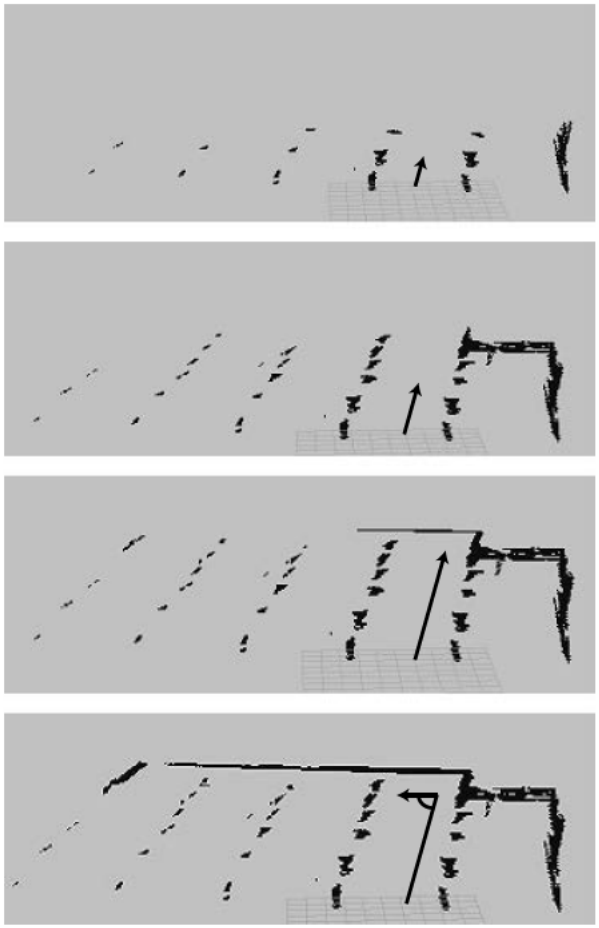

Figure 20: 2D representation of the underground parking

The second experiment, as it was mentioned before, lies in a static vehicle with a moving obstacle in front of the vehicle.

Fig. 21 shows the experiment in which a person walks in front of the vehicle and Fig. 22 shows the map produced with Rviz before the person crosses the vehicle area.

As the person (dynamic obstacle) starts to move in front of the vehicle, the sensing system detect this obstacle in real time. In order to represent this dynamic obstacle, it is shown a 3D representation with a persistence option to capture the movement. Fig. 23 shows this 3D representation at the beginning and end of the obstacle movement. As it can

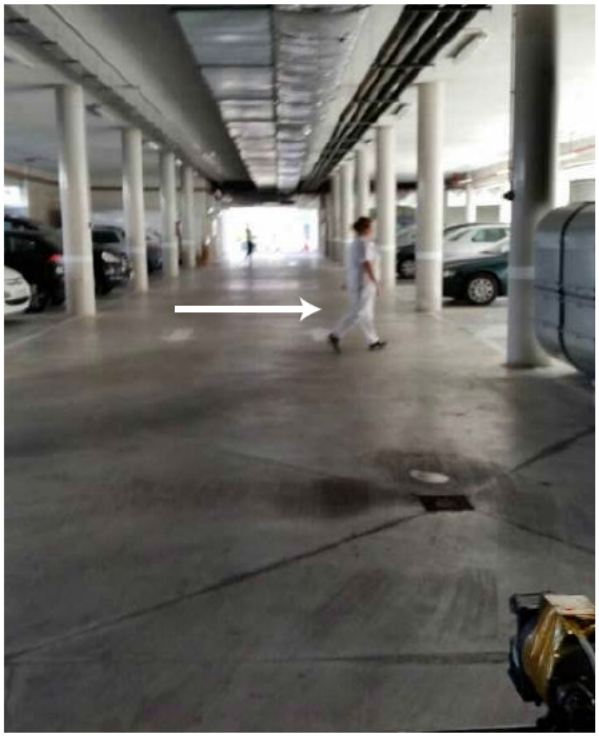

Figure 21: A person moving in front of the sensing vehicle

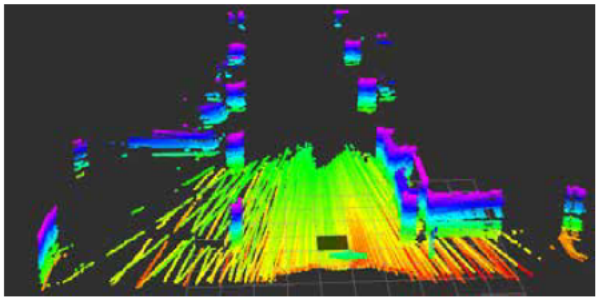

Figure 22: Map produced without any moving obstacle

be seen, the system detects the obstacle at different places, so the vehicle could stop if it was moving.

Due to the big amount of information generated by the sensor, subsampling and data reduction techniques have been used as part of the sensor processing chain. Linear and angular aperture can be selected for the sensor generated point clouds. Several algorithms for autonomy are being enabled by the sensor capabilities such as real-time ground detection and obstacle classification.

4.3. Discussion

A comparison of features with a state of the art device such as the Velodyne HDL-32E follows (see

Table 6: Comparison between the proposed system and Velodyne HDL-32E

	Proposed system using Hokuyo RLS-30LX	Velodyne HDL-32E
Horizontal and Vertical Field Of View	360° x 270°	360° x 41.3°
Laser Line Resolution	0.25°	No line
Laser scanner	Hokuyo UTM-30LX-EW	32 individual lasers
Spatial Grid Angular Resolution	From 0.25°	1.33° vertical
Accuracy (distance)	±30 mm typical	±20 mm
Measurement Range	From 0.1 m to 30 m	From 1 m to 70 m
Dimensions (H x L x W)	130 x 195 x 80 mm	150 x 86 x 86 mm + interface box
Orientation correction	Yes. Internal IMU	Yes. Internal IMU
Time for a complete 360 scan at 0.25 resolution	18 sec at 0.25° resolution. (wider resolution = faster)	No 0.25°
Laser	Pulsed laser 905 nm. Class 1	Pulsed laser 903 nm. Class 1
Price	Less than 5,000 USD	29, 900 USD

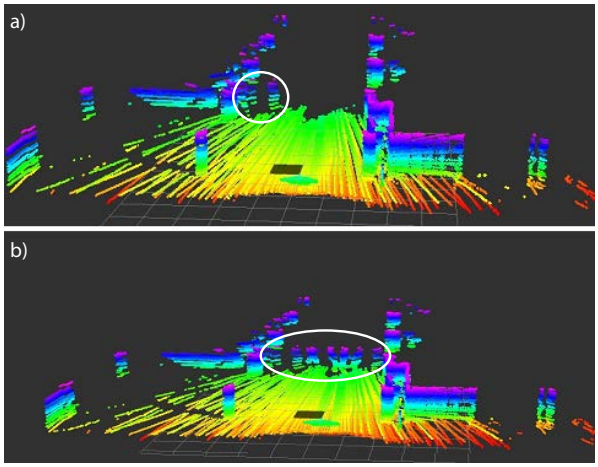

Figure 23: Map produced with the dynamic obstacle

Table 6). HDL-32E 3D LIDAR system is built from 32 individual laser points which are rotated 360° continuously thus covering a plane. Laser pointers are positioned in different angles covering a 40° vertical range with fixed 1.33° resolution. This commercial sensor has different characteristics as it rotates about the vertical axis in contrast to the horizontal front axis rotation of the sensor described in this paper. More information on the Velodyne HDL-32E sensor can be found in [33]. It achieves very good resolutions at high rotation speeds in the horizontal plane but cannot match those resolutions in the whole vertical space. Our sensor can be operated with high resolutions in the complete vertical space 270° at the expense of rotation speeds. Regarding the cost of the LIDAR systems, the proposed system costs less around 6 times less than the commercial one. Depending on the application, one or the other may be better suited for the task.

5. Conclusions

A 3D laser-based mapping system has been proposed, which includes a 2D laser sensor, and a rotation system in order to produce real time 3D maps. This proposal, which is much less expensive (under 5, 000 USD) than 3D off-the-shelf lasers (around tens of thousands of USD), has been designed for mobile unmanned ground vehicles. The proposed system is able to generate real-time point clouds in order to detect static and dynamic obstacles. Different simulation studies, which include patterns and obstacle detection, have been conducted to assess the resulting measurement data. As it was explained, the rotation speed of the sensor is key to a reliable obstacle detection, so density studies have been also made, reaching interesting results. Simulation studies show that there is not an optimal rotation speed suitable for all vehicle speeds, so the rotation speed should be adapted to the vehicle speed. Studies show that the optimal rotation speed is the minimum rotational speed which lets the scan sense all the region around the vehicle.

The proposed system can detect an obstacle of 10 cm at 10 m in front of the vehicle. Experimental results also show that it is possible to sense and produce maps of the environment in real time with high accuracy, measuring obstacles and walls with an error about 3%. Besides, the results exhibit that dynamic obstacles are also detected. Therefore, the proposed 3D sensor system provides relevant real time measurements of the surrounding for unmanned vehicles.

Acknowledgment

This work has been done with an INNPACTO program support, in the frame of ARGOS project IPT - 2012 - 0308 - 390000 (Union Europea, Fondos FEDER). It is a joint project between Robomotion

and the HCTLab, Human Computer Technology Laboratory, of Universidad Autónoma de Madrid, Spain.

References

[1] M. Montemerlo, J. Becker, S. Bhat, H. Dahlkamp, D. Dolgov, S. Ettinger, D. Haehnel, T. Hilden, G. Hoffmann, B. Huhnke, D. Johnston, S. Klumpp, D. Langer, A. Levandowski, J. Levinson, J. Marcil, D. Orenstein, J. Paefgen, I. Penny, A. Petrovskaya, M. Pflueger, G. Stanek, D. Stavens, A. Vogt, S. Thrun, Junior: The stanford entry in the urban challenge, Journal of Field Robotics 25 (9) (2008) 569–597.

[2] L. Jiang, W. Yun-Peng, C. Bai-gen, W. Jian, S. Wei, multi-sensor based vehicle autonomous navigation for vehicle infrastructure integration: Concept and simulation analysis, in: Transportation, Mechanical, and Electrical Engineering (TMEE), 2011 International Conference on, 2011, pp. 698–702. doi:10.1109/TMEE.2011.6199298.

[3] E. Thurman, J. Riordan, D. Toal, real-time adaptive control of multiple colocated acoustic sensors for an unmanned underwater vehicle, Oceanic Engineering, IEEE Journal of 38 (3) (2013) 419–432. doi:10.1109/JOE.2012.2227585.

[4] K. sub Song, P. Chu, conceptual design of future undersea unmanned vehicle (UUV) system for mine disposal, Systems Journal, IEEE 8 (1) (2014) 43–51. doi:10.1109/JSYST.2012.2210592.

[5] M. Angelopoulou, C.-S. Bouganis, vision-based egomotion estimation on FPGA for unmanned aerial vehicle navigation, Circuits and Systems for Video Technology, IEEE Transactions on 24 (6) (2014) 1070–1083. doi:10.1109/TCSVT.2013.2291356.

[6] J. Gross, Y. Gu, M. Rhudy, robust UAV relative navigation with DGPS, INS, and peer-to-peer radio ranging, Automation Science and Engineering, IEEE Transactions on 12 (3) (2015) 935–944. doi:10.1109/TASE.2014.2383357.

[7] T. Luettel, M. Himmelsbach, H.-J. Wuensche, autonomous ground vehicles — concepts and a path to the future, Proceedings of the IEEE 100 (Special Centennial Issue) (2012) 1831–1839. doi:10.1109/JPROC.2012.2189803.

[8] M. Atia, S. Liu, H. Nematallah, T. Karamat, A. Noureldin, integrated indoor navigation system for ground vehicles with automatic 3D alignment and position initialization, Vehicular Technology, IEEE Transactions on 64 (4) (2015) 1279–1292. doi:10.1109/TVT.2015.2397004.

[9] F. Bonin-Font, A. Ortiz, G. Oliver, visual navigation for mobile robots: A survey, Journal of intelligent and robotic systems 53 (3) (2008) 263–296.

[10] G. Desouza, A. Kak, vision for mobile robot navigation: a survey, Pattern Analysis and Machine Intelligence, IEEE Transactions on 24 (2) (2002) 237–267. doi:10.1109/34.982903.

[11] D. Gonzalez-Arjona, A. Sanchez, F. López-Colino, A. de Castro, J. Garrido, simplified occupancy grid indoor mapping optimized for low-cost robots, ISPRS International Journal of Geo-Information 2 (4) (2013) 959–977.

[12] A. Ward, A. Jones, A. Hopper, a new location technique for the active office, Personal Communications, IEEE 4 (5) (1997) 42 –47. doi:10.1109/98.626982.

[13] N. B. Priyantha, A. K. Miu, H. Balakrishnan, S. Teller, the cricket compass for context-aware mobile applications, in: Proceedings of the 7th annual international conference on Mobile computing and networking, MobiCom '01, ACM, New York, NY, USA, 2001, pp. 1–14. doi:http://doi.acm.org/10.1145/381677.381679.

[14] A. Sanchez, A. de Castro, S. Elvira, G. G. de Rivera, J. Garrido, Autonomous indoor ultrasonic positioning system based on a low-cost conditioning circuit, Measurement 45 (3) (2012) 276 – 283.

[15] S. Elvira, A. de Castro, J. Garrido, ALO: An ultrasound system for localization and orientation based on angles, Microelectronics Journal 44 (10) (2013) 959 – 967.

[16] P. Cory, H. R. Everett, T. A. Heath-Pastore, Radar-based intruder detection for a robotic security system, in: Photonics East (ISAM, VVDC, IEMB), International Society for Optics and Photonics, 1999, pp. 62–72.

[17] R. Mautz, S. Tilch, survey of optical indoor positioning systems, in: Indoor Positioning and Indoor Navigation (IPIN), 2011 International Conference on, 2011, pp. 1–7. doi:10.1109/IPIN.2011.6071925.

[18] Nasa: Seventeen cameras on curiosity.
URL `http://www.nasa.gov/mission_pages/msl/multimedia/malin-4.html`

[19] Velodyne products.
URL `http://velodynelidar.com/lidar/lidar.aspx`

[20] Sick products.
URL `http://www.sick.com/us/en-us/home/products/product_portfolio/Pages/product_portfolio.aspx`

[21] T. Stoyanov, R. Mojtahedzadeh, H. Andreasson, A. J. Lilienthal, Comparative evaluation of range sensor accuracy for indoor mobile robotics and automated logistics applications, Robot. Auton. Syst. 61 (10) (2013) 1094–1105.

[22] International Electrotechnical Commission and American National Standards Institute, IEC 60529: Degrees of protection provided by enclosures (IP code).

[23] A. D. Chambers, S. Achar, S. T. Nuske, J. Rehder, B. M. Kitt, L. J. Chamberlain, J. Haines, S. Scherer, S. Singh, Perception for a river mapping robot, in: Proceedings of the 2011 IEEE/RSJ International Conference on Intelligent Robots and Systems (IROS '11), 2011.

[24] T. Yoshida, K. Irie, E. Koyanagi, M. Tomono, A sensor platform for outdoor navigation using gyro-assisted odometry and roundly-swinging 3d laser scanner, in: Intelligent Robots and Systems (IROS), 2010 IEEE/RSJ International Conference on, 2010, pp. 1414–1420.

[25] M. Matsumoto, S. Yuta, 3d laser range sensor module with roundly swinging mechanism for fast and wide view range image, in: Multisensor Fusion and Integration for Intelligent Systems (MFI), 2010 IEEE Conference on, 2010, pp. 156–161.

[26] A. Djuricic, B. Jutzi, Supporting UAVs in low visibility conditions by multiple-pulse laser scanning devices, The International Archives of the Photogrammetry, Remote Sensing and Spatial Information Sciences 1 (2013) W1.

[27] Z. Chong, B. Qin, T. Bandyopadhyay, M. Ang, E. Frazzoli, D. Rus, Synthetic 2D LIDAR for precise vehicle localization in 3D urban environment,

in: Robotics and Automation (ICRA), 2013 IEEE International Conference on, 2013, pp. 1554–1559. doi:10.1109/ICRA.2013.6630777.

[28] Hokuyo LX30.
URL http://www.hokuyo-aut.jp/02sensor/07scanner/download/pdf/UTM-30LX-EW_spec_en.pdf

[29] Gazebo robotics simulator.
URL http://gazebosim.org/

[30] Robotic Operating System.
URL http://www.ros.org

[31] Rviz visualization package.
URL http://wiki.ros.org/rviz

[32] Octovis visualization package.
URL http://wiki.ros.org/octovis

[33] C. Velodyne Lidar Inc. Morgan Hill, HDL-32E High Definition LiDAR Sensor. Users Manual and Programming Guide (July 2015).